BIOCHEMISTRY
including biophysical chemistry & molecular biology

Accelerated Publication

pubs.acs.org/biochemistry

A Novel Soluble Peptide with pH-Responsive Membrane Insertion

Vanessa P. Nguyen, Daiane S. Alves, Haden L. Scott, Forrest L. Davis, and Francisco N. Barrera*

Department of Biochemistry and Cellular and Molecular Biology, University of Tennessee, Knoxville, Tennessee 37996, United States

ABSTRACT: Several diseases, such as cancer, are characterized by acidification of the extracellular environment. Acidosis can be employed as a target to specifically direct therapies to the diseased tissue. We have used first principles to design an acidity-triggered rational membrane (ATRAM) peptide with high solubility in solution that is able to interact with lipid membranes in a pH-dependent fashion. Biophysical studies show that the ATRAM peptide binds to the surface of lipid membranes at pH 8.0. However, acidification leads to the peptide inserting into the lipid bilayer as a transmembrane α-helix. The insertion of ATRAM into membranes occurs at a moderately acidic pH (with a pK of 6.5), similar to the extracellular pH found in solid tumors. Studies with human cell lines showed a highly efficient pH-dependent membrane targeting, without causing toxicity. Here we show that it is possible to rationally design a soluble peptide that selectively targets cell membranes in acidic environments.

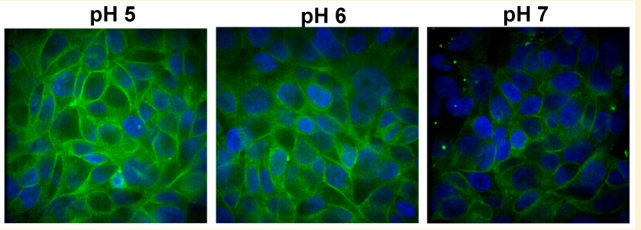

Targeted therapies hold great promise for the treatment of numerous diseases. This class of therapies often relies on the expression of a molecular target in the diseased cell. However, drug resistance frequently results from mutation, downregulation, or signaling cross-talk of the molecular target.[1] The successful targeted therapies of the future will benefit by being directed instead at a prevalent feature of the disease. Several pathological states, such as cancer,[2] ischemia, and inflammation, have a significantly disrupted pH balance resulting in acidosis. In the case of cancer, alterations in the metabolism and physiology of solid tumors cause extracellular acidosis.[3,4] Strikingly, it has been recently shown that acidosis favors tumor aggressiveness. In particular, acidity enhances metastasis[5] and local invasion[6] and plays an immunosuppressive role.[7] Therefore, technologies that target therapeutic cargos to acidic tissues might be of general use for fighting acidic diseases such as cancer. Furthermore, as a consequence of the competitive advantage acidosis confers to cancer cells, therapies targeting acidosis might be less susceptible to resistance.

Peptides are attractive molecules for the delivery of cargo to acidic diseased tissues. Peptides show high efficacy, selectivity, and safety[8] and are also naturally endowed to respond to acidification, by means of the titration of the acidic residues aspartate and glutamate. Here, we report the rational design of an acidity-triggered rational membrane (ATRAM) peptide, which responds to acidification by inserting into the membrane of tumor cells.

EXPERIMENTAL PROCEDURES

Liposome Preparation. Stocks of POPC (1-palmitoyl-2-oleoyl-*sn*-glycero-3-phosphocholine) (Avanti Polar Lipids, Inc.) were prepared in chloroform. Appropriate aliquots of lipids were dried first with argon gas and then under a vacuum overnight. The dried lipid films were rehydrated using 10 mM NaP_i buffer (pH 8.0). Large unilamellar vesicles (LUVs) were prepared with a Mini-Extruder (Avanti Polar Lipids, Inc.) through a 100 nm pore size membrane (Whatman).

Peptide Preparation and Conjugation. Peptides were prepared by FMOC solid phase synthesis and purified by reverse phase high-performance liquid chromatography to >95% purity. For biophysical experiments, the ATRAM peptide was labeled at the N-terminus with NBD (nitrobenzoxadiazole) using NBD-X succimidyl ester or rhodamine (5,6-carboxytetramethylrhodamine, succinimidyl ester, Anaspec). For microscopy, ATRAM and pHLIP were labeled at the N-terminus with BODIPY FL-X, which contains a seven-atom spacer between the dye and the conjugation point. Free dyes were removed by gel filtration through a PD-10 column, and matrix-assisted laser desorption ionization time of flight was employed to determine that a single dye molecule was bound per peptide molecule. The expected and observed molecular mass ($M + H^+$) values were 3623.1 and 3624.0, respectively.

NBD Lipid Binding Assay. The assay was performed as described elsewhere.[9] Briefly, lyophilized samples of ATRAM-NBD were rehydrated in 10 mM NaP_i (pH 8) at a final concentration of 1 μM and incubated with increasing concentrations of POPC LUVs. Emission spectra were recorded on a Photon Technology International Quanta Master fluorometer. The appropriate lipid background was subtracted in all cases. Data were analyzed by following the fluorescence intensity change at 540 nm. Data were fitted with OriginLab using eq 1:

$$F_o + F_{max} \times (K_p x)/(55.3 + K_p x) \quad (1)$$

where F_o is the initial fluorescence intensity, F_{max} is the maximal fluorescence intensity, x is the lipid concentration, and 55.3 is the molar concentration of water. Equation 1 was used to

Received: July 29, 2015
Published: October 24, 2015

DOI: 10.1021/acs.biochem.5b00856
Biochemistry 2015, 54, 6567−6575

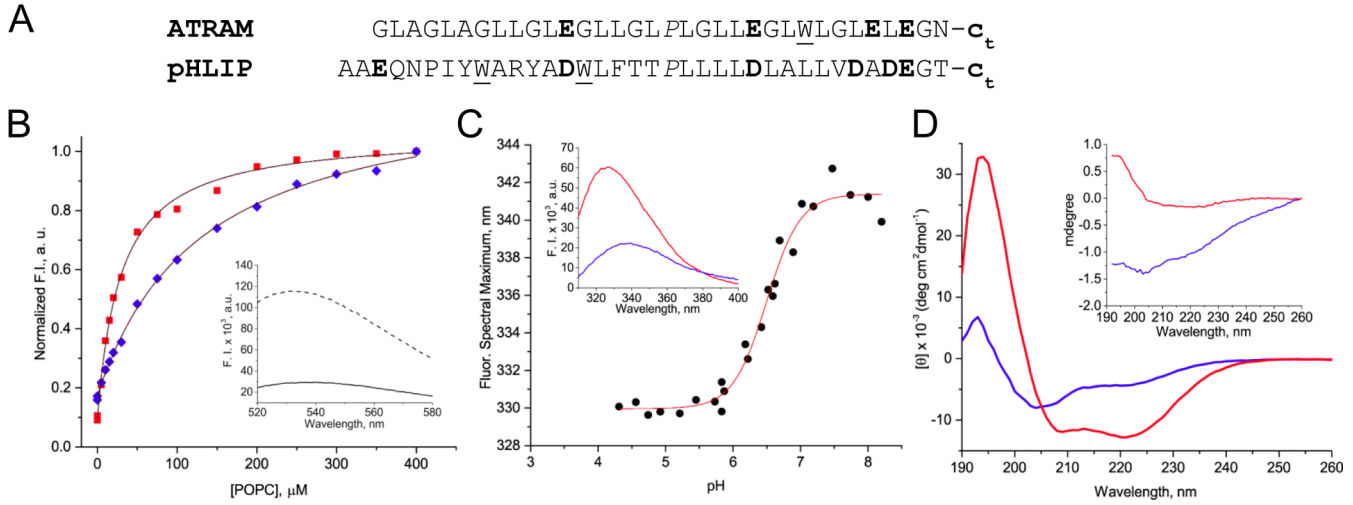

Figure 1. Biophysical characterization of the ATRAM peptide. (A) Sequence of ATRAM. The acidic moieties, glutamic acid and free C-terminus, are shown in bold; proline is shown in italics, and the single tryptophan introduced for intrinsic fluorescence experiments is underlined. The sequence of pHLIP is shown for comparison. (B) POPC binding assay of ATRAM-NBD (1 μM) at pH 8.0 (blue symbols) and pH 6.0 (red symbols). The fluorescence intensities were normalized to the maximal value. Curves were fitted to eq 1 (black lines). The inset shows the NBD fluorescence spectra at 10 and 400 μM POPC (solid and dashed lines, respectively) at pH 8. (C) Representative pH titration curve obtained by monitoring the tryptophan fluorescence spectral maximum of ATRAM in POPC (n = 4). The line is the fitting to eq 2, to determine the pK and the slope of the titration. The slope obtained for ATRAM (1.6 ± 0.4) was similar to the value for the pHLIP in the same lipid (1.2 ± 0.3[68]). The inset shows the tryptophan fluorescence spectra of ATRAM in POPC LUVs at pH 4.3 (red line) and pH 7.7 (blue line). (D) Circular dichroism spectra of ATRAM in POPC at different pH values. Data shown for the ATRAM peptide with POPC vesicles at pH 7.9 and 4.1 (blue and red lines, respectively). The inset shows the OCD spectra in POPC at pH 4.1 (red line) and pH 8.0 (blue line).

determine the partition coefficient, K_p, defined as the ratio of concentrations of a compound in a mixture of two phases.

Intrinsic Fluorescence Spectroscopy. For the pH titration experiments, 1 μM ATRAM was incubated for at least 1 h with POPC LUVs to reach a 1:200 molar ratio. The pH of the samples was changed accordingly with 100 mM buffers (sodium acetate, MES, or HEPES). Tryptophan fluorescence emission spectra were recorded at an excitation wavelength of 280 nm. Measurements were performed on a Photon Technology International Quanta Master fluorometer. The appropriate lipid background was subtracted. The data were analyzed by monitoring the spectral maxima, which were then fitted to determine the pK, using eq 2:

$$[F_a + F_b \times 10^{m(\mathrm{pH}-\mathrm{p}K)}]/[1 + 10^{m(\mathrm{pH}-\mathrm{p}K)}] \quad (2)$$

where F_a is the acidic baseline, F_b is the basic baseline, m is the slope of the transition, and pK is the midpoint of the curve.

Circular Dichroism. Measurements were performed on a Jasco J-815 spectropolarimeter at 25 °C. Peptide was incubated with lipid in 10 mM NaP_i (pH 8.0) or 10 mM sodium acetate (pH 4.1). Samples were prepared as described above. The lipid:peptide ratio was 100:1 with a final peptide concentration of 5 μM. The appropriate lipid backgrounds were subtracted.

Oriented Circular Dichroism. OCD was performed as described elsewhere.[9] Briefly, the Langmuir–Blodgett method was used to form a monolayer on a demountable quartz cuvette with a KSV NIMA trough. A peptide/lipid solution (1:50 molar ratio) at pH 4 or 8 was incubated with the monolayer under 100% humidity to complete vesicle fusion to obtain supported bilayers. The OCD spectrum was measured on a Jasco J-815 spectropolarimeter, and appropriate backgrounds were subtracted.

Calcein Leakage Assay. A dried POPC lipid film was rehydrated with 50 mM calcein in 10 mM HEPES and 50 mM EDTA (pH 8). Large unilamellar vesicles were prepared as described above. Free calcein was removed by gel filtration through a PD-10 column. Peptide was added to the calcein/LUV suspensions at different concentrations to achieve final peptide:lipid molar ratios of 0.0025–0.5%. After incubation at room temperature for 30 min, calcein leakage was tracked by measuring fluorescence using a Synergy 2 microplate reader (BioTek) at an excitation wavelength of 485 nm and an emission wavelength of 528 nm. Complete calcein release was reached by adding 20% Triton X-100.

FRET Oligomerization Assay. Lyophilized samples of ATRAM, ATRAM-NBD (donor), and ATRAM-Rho (acceptor) were rehydrated in 10 mM NaP_i buffer (pH 8). The donor was held at 0.1 μM, and the acceptor was used in a range of concentrations from 0 to 0.5 μM. Unlabeled peptide was added to keep the final peptide concentration constant at 2 μM. To minimize scattering, polarizers were employed: excitation polarizers set to 90° and emission polarizers set to 0°.[10,11] Lipid blanks were subtracted in all cases. The final lipid:peptide ratio was 200:1.

Vesicle Fusion Assay. FRET was used to determine the amount of vesicle fusion induced by ATRAM. PE-Rho and PE-NBD were from Avanti Polar Lipids. Vesicles containing 99 mol % POPC, 0.5 mol % PE-NBD (donor), and 0.5% PE-Rho (acceptor) were prepared like POPC vesicles. The final ATRAM concentration was 1.9 μM. Unlabeled POPC vesicles were added to vesicles containing labeled lipids in the presence of ATRAM. POPC vesicles containing labeled lipids were measured separately to determine the maximal amount of energy transfer. Triton X-100 (final concentration of 0.7%) was added to samples containing POPC vesicles with labeled lipids to inhibit the FRET signal to determine the smallest amount of energy transfer. Appropriate lipid blanks were subtracted from each sample to correct for the effect of light scattering caused by lipids. POPC vesicles containing 0.5 mol % PE-Rho in the absence and presence of Triton X-100 were used to determine

DOI: 10.1021/acs.biochem.5b00856
Biochemistry 2015, 54, 6567–6575

the correction factor to account for the disturbance in the emission spectra caused by the addition of Triton X-100. The percent fusion was calculated using eq 3:

$$\left(\frac{\text{sample} - \text{control}}{\text{Triton} - \text{control}}\right) \times 100 \quad (3)$$

where Sample contains ATRAM, labeled vesicles, and unlabeled vesicles; Control is identical but without ATRAM; and Triton is POPC containing labeled lipids after the addition of Triton X-100. All intensity values were measured at 594 nm.

Cell Binding Assays: Plate Reader and Confocal Microscopy. A375 and H358 cells (ATCC) were washed twice with phosphate-buffered saline supplemented with 1 mM $MgCl_2$ and 100 μM $CaCl_2$ (PBS^{++}) and incubated with 2 μM peptide (ATRAM-BODIPY or pHLIP-BODIPY) for 5 min, followed by an incubation of 90 s with PBS^{++} containing 10 mM dextrose (Sigma-Aldrich) at different pHs (5, 6, and 7). Cells were then washed once in the same buffer and subsequently fixed with 4% paraformaldehyde for 30 min. Plate reader binding assays were performed using cells cultured in a 96 black collagen-coated plate (Corning), and the fluorescence intensity was detected at 488 nm in a plate reader (Synergy 2, Biotek). The quantification analysis is a result of three independent experiments performed in triplicate. Cell imaging was performed at room temperature using an inverted Olympus Ix83 microscope with a confocal laser scanning VT-HAWK system equipped with a 60 × 1.35NA objective from Visitech International, running metamorph, and a Hamamatsu EM-CCD camera (model C9100-13). Contrast and brightness settings were chosen so that all pixels were in the linear range. Images from different channels were overlaid using ImageJ.

Cell Proliferation Assay (MTS). Cell viability was measured using the CellTiter 96 Aqueous One Solution. Briefly, cells were seeded (10^4 cells/well) 2 days prior the experiments on a 96-well plate, exposed to vehicle (CT) or ATRAM at different concentrations (0.5, 1, and 2 μM), and incubated for 24 h. The results are representative of three independent experiments, performed in quadruplicate. The inhibition of cell proliferation was expressed as the percentage of vehicle control.

RESULTS

The potential of peptides for targeting acidosis is exemplified by the pH-low insertion peptide (pHLIP). The pHLIP, developed in the laboratories of Engelman, Reshetnyak, and Andreev, is a soluble peptide that binds to membranes in a mostly unstructured conformation at neutral pH. Upon acidification, the pHLIP undergoes a conformational change, forming a transmembrane (TM) α-helix as it spans the membrane.[12−14] Several residues important for pHLIP properties, such as the acidic groups responsible for the pH dependency, and a central proline residue that increases solubility,[15] were included in the sequence of the ATRAM peptide (Figure 1A). Glutamates were chosen over aspartates, because they have higher pK_a values, more appropriate for the targeting of acidic diseased tissues. For the rest of the ATRAM sequence, residues were selected to yield an overall hydrophobicity similar to that of pHLIP[16] by balancing the more hydrophobic leucine with the less hydrophobic alanine and glycine (Gly). Gly was preferred over alanine because, interestingly, the conformational propensity of Gly is strongly dependent on the environment. Hence, while in solution Gly destabilizes the secondary structure found in aggregates, in membranes Gly favors the formation of helices.[17,18] Hence, we believe that Gly minimizes aggregation in solution without disrupting α-helix formation in membranes. Finally, a single tryptophan residue was introduced into the ATRAM peptide to perform intrinsic fluorescence evaluation of the properties of the peptide.

We found that ATRAM readily dissolved in aqueous buffer (see details below), allowing us to evaluate the interaction with lipids. We first studied the binding of the ATRAM peptide to synthetic vesicles. As a lipid of choice, we selected POPC, because its phosphatidylcholine headgroup is the most abundant in the eukaryotic plasma membrane,[19,20] while also containing saturated and unsaturated fatty acids. To accurately measure the binding of ATRAM to POPC LUVs, we labeled the peptide with an environmentally sensitive fluorescent probe, NBD.[9] We observed that incubation with POPC at pH 8.0 caused a large increase in the fluorescence of the NBD conjugated to ATRAM (Figure 1B, blue symbols), as well as a blue-shift in the spectral maximum (Figure 1B, inset). Both spectral changes are characteristic of dehydration of the NBD group,[21−23] suggesting that ATRAM binds to lipid membranes. We next studied whether the interaction of ATRAM with membranes was pH-responsive, as required for the targeting of diseased cells in acidic environments. For this purpose, we monitored the intrinsic fluorescence of the single tryptophan residue (Figure 1A, underlined). A pH titration experiment was performed for samples of ATRAM incubated with POPC. Upon acidification, we observed a blue-shift in the emission spectrum from ∼340 to ∼330 nm and a large increase in fluorescence (Figure 1C). From the obtained spectral maximum curve, we determined the membrane insertion pK, defined as the midpoint of the sigmoid, with a value of 6.51 ± 0.09. The blue-shift of the intrinsic fluorescence of ATRAM indicated that at acidic pH values the tryptophan in the peptide was more deeply buried in the membrane than at neutral pH, suggesting a tighter interaction. To evaluate how membrane affinity could depend on pH, we repeated the NBD lipid binding experiments at pH 6.0 (Figure 1B, red symbols). We observed that ATRAM bound more readily to POPC at pH 6.0 than at pH 8.0. We analyzed the binding isotherms to determine the partition coefficient, K_p, with values of $(5.5 \pm 2.5) \times 10^5$ at pH 8.0 and $(16.5 \pm 2.5) \times 10^5$ at pH 6.0, demonstrating that ATRAM binds to membranes with higher affinity under acidic conditions.

To study the conformation of ATRAM in the membrane, we employed circular dichroism (CD) spectroscopy (Figure 1D). At pH 8 (blue line), the CD spectrum showed a minimum of 204 nm and a small shoulder at 222 nm. These spectral features are typically observed for partially disordered peptides with some helical content.[24] Interestingly, at acidic pH (red line), the helical content increased, as shown by the large decrease in the magnitude of the signal at 222 nm, the shift of the minimum from 204 to 208 nm, and the large increase in ellipticity at 195 nm. We performed a rough quantification of the helical content at both pH values. By considering for 100% α-helix a $[\Theta]$ of −36000 deg cm^2 dmol^{-1} residue^{-1},[25] we estimated that the helical content increased from ∼12% at pH 8 to ∼37% at pH 4. However, the membrane alignment of the helical region of ATRAM was not known. To gain information about the helical orientation with respect to the plane of the bilayer, we prepared supported bilayers and performed oriented CD (OCD) experiments.[26,27] When α-helices span the membrane, the OCD spectrum characteristically displays a

DOI: 10.1021/acs.biochem.5b00856
Biochemistry 2015, 54, 6567−6575

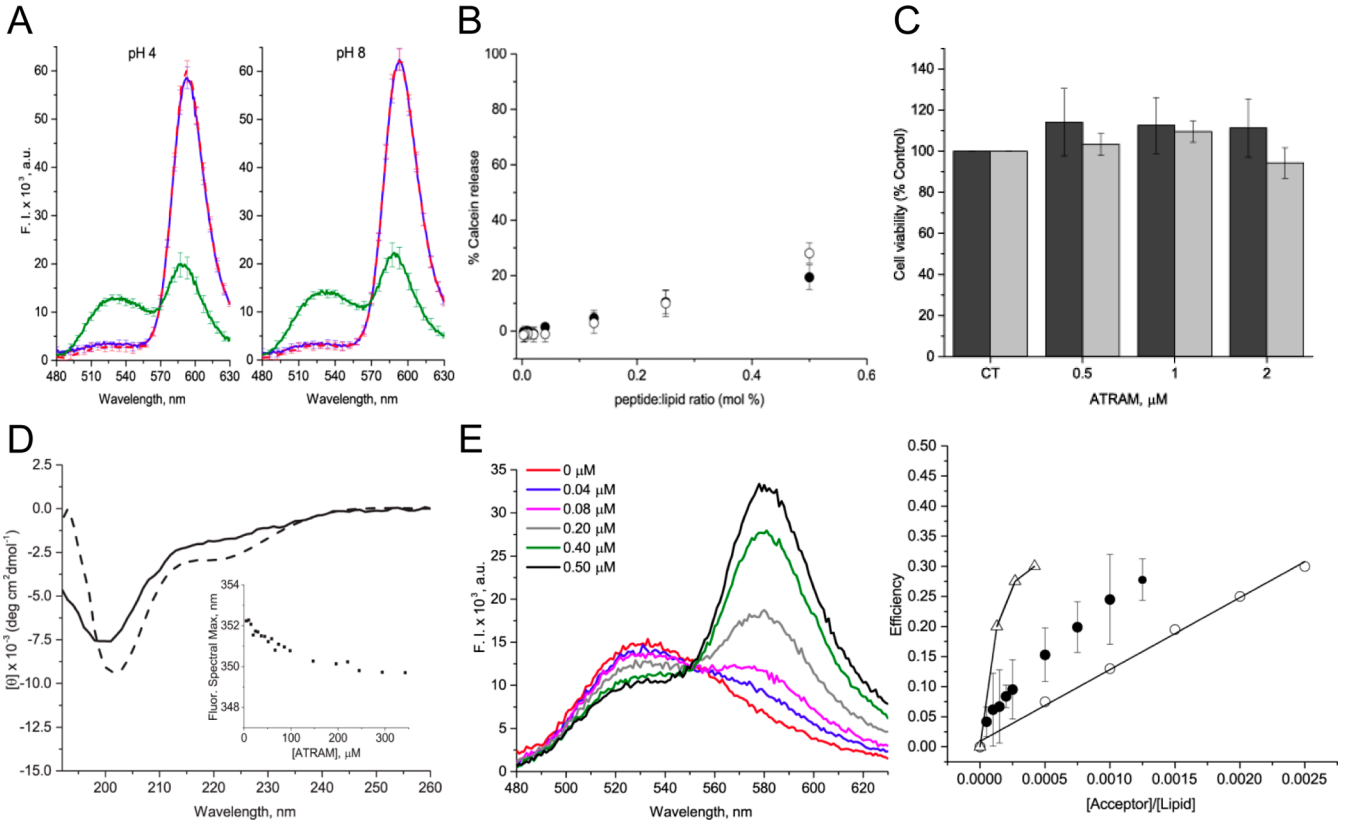

Figure 2. Membrane interaction and self-assembly of the ATRAM peptide. (A) FRET vesicle fusion assay. The effect of ATRAM on vesicle fusion/hemifusion was determined at pH 4.0 (TM state, left) and pH 8.0 (interfacial state pH, right). The curves show data from vesicles in the absence of peptide (dashed red line), in the presence of peptide (blue line), and membrane disruption by Triton X-100 (green line). (B) Comparison of the effect of ATRAM and pHLIP on membrane leakage. The fluorescence intensity of calcein encapsulated in POPC vesicles was monitored after the addition of peptide (0.0025−0.5 mol %) in 10 mM NaP_i (pH 8.0): (○) ATRAM and (●) pHLIP (n = 3). (C) MTS cell viability assay performed in the presence of ATRAM for two different human cell lines: A358 (black) and H358 (gray). Data show the cell viability at increasing ATRAM concentrations compared to that of nontreated control cells (CT). Results are the means of three independent experiments. No statistically significant cell toxicity was observed at any of the ATRAM concentrations. (D) Solubility studies of ATRAM in a 10 mM NaP_i solution (pH 7.9) at increasing concentrations. CD spectra are shown for 5 and 200 μM peptide (solid and dashed lines, respectively). The inset shows the fluorescence spectral maxima of ATRAM at increasing concentrations. (E) The oligomerization of the TM state of ATRAM was studied using FRET. The left panel shows the fluorescence spectra. Increasing amounts of ATRAM-Rho (acceptor) were added to the samples, and the intensity of the FRET signal increased through quenching of ATRAM-NBD (donor), which was kept at a constant concentration (n = 3). The right panel shows the calculated FRET efficiency values for ATRAM (●). The line shows the theoretical FRET efficiency values expected for random encounters of a TM monomeric peptide (○).[51,69] To guide the discussion, we show FRET data for oligomeric helix α5 of Cry1Ac of *Bacillus thuringiensis*[35] (△).

broad minimum at ∼220−225 nm and a shoulder with positive ellipticity at 190−195 nm. These characteristics were observed at acidic pH (Figure 1D, inset), indicating that ATRAM adopts a TM orientation at low pH. On the other hand, the OCD spectrum of an α-helix lying parallel to the plane of the membrane shows a much more intense negative signal and more clearly resolved minima at ∼205 and ∼222 nm, which are similar to our data at pH 8. The OCD data thus indicate that ATRAM lies parallel to the membrane plane at neutral pH, but it responds to acidification by inserting as a TM α-helix.

Toxicity to Healthy Cells Poses a Significant Concern in the Design of Membrane Active Peptides. Numerous examples of peptides that disrupt membranes by formation of pores or membrane solubilization or fusion exist.[28−32] To rule out the possibility that ATRAM might disrupt the integrity of cell membranes, we performed different assays on lipid vesicles and cells. We studied first whether ATRAM induced vesicle fusion or hemifusion by performing a FRET assay with two different fluorescently labeled lipids. Figure 2A shows that ATRAM induced no statistically significant fusion or hemifusion of POPC LUVs, neither at pH 8.0 nor at pH 4.0. We also performed an assay to study vesicle leakage of encapsulated calcein. A previous report showed that pHLIP caused only minor calcein release, in agreement with data indicating that membrane integrity is not significantly disrupted by pHLIP.[33] We performed a similar assay comparing pHLIP and ATRAM (Figure 2B). We observed that the signal was similar for both peptides at most peptide:lipid ratios, and only slightly higher for ATRAM at the highest concentration. Intrigued by the leakage results in synthetic vesicles, we performed an assay to study whether ATRAM disrupted the membrane of cells. We performed a cell viability assay in two different cell lines (Figure 2C) that shows that ATRAM does not cause cell toxicity. This result indicates that ATRAM did not disrupt cellular membranes at any of the concentrations assayed.

To study whether the ATRAM peptide was capable of self-assembly, we performed oligomerization assays in solution and in the membrane-inserted state at pH 4. Protein oligomerization is typically associated with a folded state, because protein−protein interfaces tend to adopt a well-defined conformation.

DOI: 10.1021/acs.biochem.5b00856
Biochemistry 2015, 54, 6567−6575

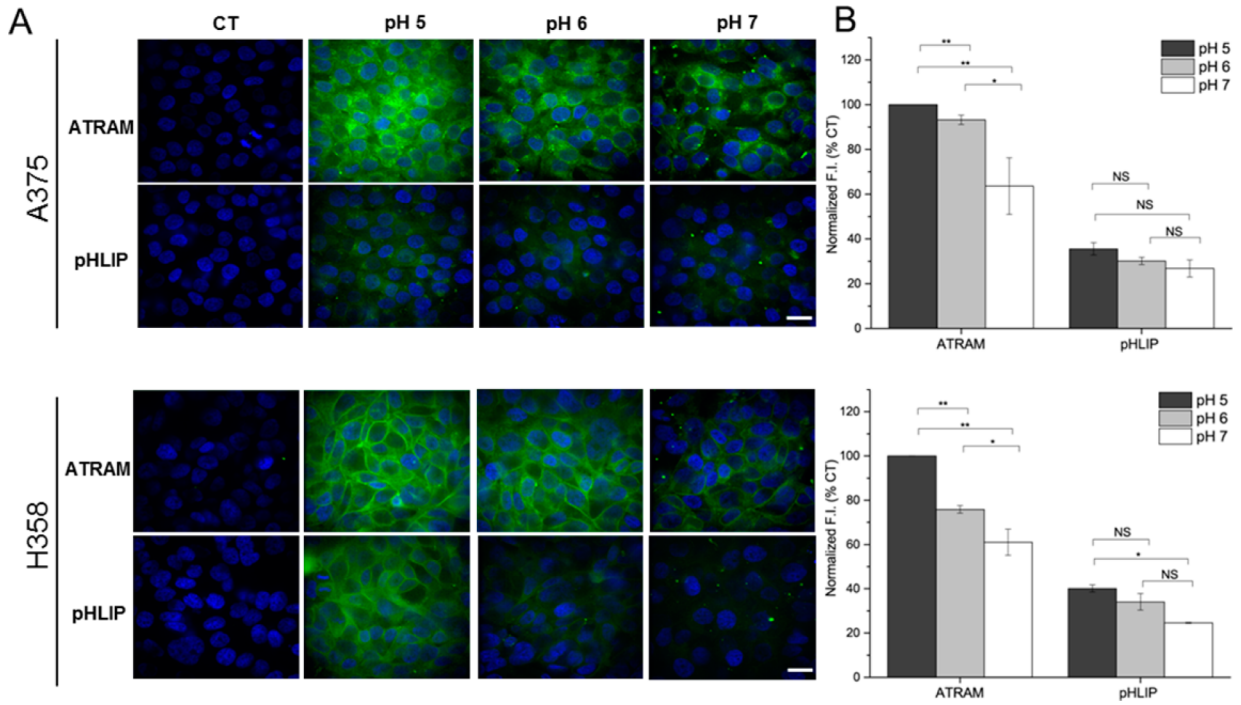

Figure 3. pH-dependent interaction of ATRAM with cells. (A) Confocal images of ATRAM-BODIPY and pHLIP-BODIPY in two cell lines: A375 (top row) and H358 (bottom row). Images compare the pH-dependent targeting of cells by ATRAM and pHLIP. The gain employed was identical in all panels and selected to avoid saturation of the ATRAM pH 5 samples. Typical results from one of three experiments are presented. The bar is 20 μm. (B) Plate reader quantification at pH 5.0 (black), pH 6.0 (gray), and pH 7.0 (white). Data were normalized to the maximal fluorescence detected in each experiment. Results are means of three independent experiments, and the error bars show the standard deviation. Student's *t* test: NS, nonsignificant; $*p < 0.05$; and $**p < 0.01$.

We first employed CD to determine the structure adopted by the ATRAM peptide in solution. The CD spectrum at 5 μM displays a minimum at ~200 nm, indicating that the peptide is largely unstructured. However, a small shoulder at 222 nm suggests minor helical structure (Figure 2D). Increasing the peptide concentration to 200 μM caused only small CD changes, which suggest a minor increase in helicity from ~5 to ~10%.[25] We obtained further insights by monitoring the intrinsic fluorescence of ATRAM at increasing concentrations (Figure 2D, inset). At all concentrations, the sole tryptophan in the peptide was highly solvated, as indicated by the spectral maximum between 350 and 352 nm. Nonetheless, a small, seemingly nonlinear shift was observed, compatible with the presence of some concentration-dependent peptide self-association in solution. However, because the peptide at 200 μM is largely unfolded, and the tryptophan is highly hydrated, we favor the possibility that the monomer is the main species present even at high concentrations. Finally, we performed a FRET experiment to characterize whether ATRAM self-associated in the TM form (Figure 2E). We observed FRET efficiency values higher than those expected for a monomer (○), suggesting that ATRAM is in an oligomeric state. Figure 2E shows data obtained under similar conditions for helix α5 of Cry1Ac (△), postulated to form a transmembrane tetramer.[34,35] The FRET of ATRAM was significantly lower, suggesting that the ATRAM peptide assembles into a small oligomeric species, a dimer or a trimer.

Our data showed that ATRAM interacted in a pH-dependent fashion with synthetic vesicles. However, it was critical to establish whether the desirable properties of the peptide were maintained in cells. The ability of ATRAM to bind to cultured cells was studied first by fluorescence microscopy for two different human cancer cell lines, A375 (malignant melanoma) and H358 (bronchioalveolar carcinoma) (Figure 3A). To explore whether ATRAM showed potential for targeting acidosis, experiments at decreasing pH values were performed in parallel with the well-established pHLIP.[13,14,36,37] We labeled both peptides with a fluorescent dye, BODIPY FL-X, to monitor their cellular distribution. After a brief incubation with the peptides, cells were rinsed with solutions of different pH values, and the fluorescent signal was evaluated. Interestingly, ATRAM was able to bind to cells in a pH-dependent fashion, with stronger cell interaction at acidic pH values. To quantify the association with cells, the total fluorescence signal for the bound peptides was measured in a plate reader assay. Figure 3B depicts the quantification of the pH-dependent interaction with the two cell lines. The results indicated that the overall level of binding of ATRAM to both cell lines was higher than for pHLIP. Furthermore, it was evident that ATRAM targeted more efficiently cells in acidic environments. Taken together, our results indicate that ATRAM is capable of targeting cells, and this ability is significantly greater under acidosis, without causing toxicity.

■ DISCUSSION

We are currently in the midst of a golden era in the protein design field. A substantial number of exciting successes have been recently achieved to engineer protein functions and structures employing different computational tools.[38,39] For example, the Rosetta method allows the *de novo* design of certain small soluble and membrane proteins with different functions.[40,41] In the membrane protein field, DeGrado and co-workers have been able to computationally design transmembrane peptides that inhibit integrins[42] as well as to create

DOI: 10.1021/acs.biochem.5b00856
Biochemistry 2015, 54, 6567−6575

membrane helical bundles of diverse functionalities.[43,44] However, synthetic biological elements can be created without computationally intensive methodologies. Protein design can also be undertaken by employing first principles and guided by experimental data. A salient example is the maquette method of the Dutton laboratory, which allows engineering of an astounding variety of oxidoreductase functionalities into four-helix bundles.[45] Upon application to membrane proteins, it is also worth mentioning the pioneering work in which synthetic peptides were assembled into membranes forming an ion channel.[46]

Here we wanted to design *de novo* a water-soluble peptide whose interaction with lipid membranes was controlled by pH. Despite its small size, designing this kind of molecule is challenging, because the peptide is required to be stable in environments of very different hydrophobicities (aqueous solution and the membrane).[47] Furthermore, acidification should efficiently trigger insertion into the membrane. While the pHLIP has been successfully applied for imaging[48] and drug delivery across membranes[49,50] for various solid tumors, several features potentially restrict its use. These include modest targeting of mildly acidic tumors[48] and a relatively strong tendency to aggregate.[51] To overcome these limitations, sequence refinement of pHLIP is desirable.[52] However, progress has been hindered as a result of the lack of solubility commonly found in single mutants of pHLIP.[53] The peptide described herein was designed to fill this need. Learning from pHLIP, we designed the ATRAM peptide with a sequence that was only 23.5% identical to the sequence of pHLIP.

The ATRAM peptide is highly soluble in pH 8 buffer, where it remains in a largely unstructured conformation. As projected, it is capable of binding to lipid vesicles at neutral pH, and under acidic conditions, it forms an α-helix that aligns perpendicular to the membrane plane. We hypothesize that a feature important for understanding the mechanism of ATRAM is the increase in helical content associated with the coupled membrane insertion and folding (Figure 1D). In the surface-bound, preinserted state, few peptide backbone hydrogen bonds are formed. Hydrogen bonds are more energetically favored in the low-dielectric membrane core.[54] Therefore, formation of backbone hydrogen bonds integral to a TM helix will drive membrane insertion of ATRAM. The OCD data indicate that ATRAM forms a TM α-helix at acidic pH. The magnitude of the CD signal suggests that the TM state of ATRAM includes long disordered stretches. It is likely that those correspond to the two ends of the sequence, while the central region spans the membrane. Interestingly, quantification of the CD α-helical content would suggest that the TM region of ATRAM might be shorter than the 20 residues typically found in TM domains.[54,55] Nonetheless, quantification of secondary structure percentages by CD is often associated with significant errors.[56] However, we are confident that the ellipticity at 222 nm of ATRAM is compatible with a transmembrane span, because a very similar CD spectrum is observed under conditions where pHLIP forms a *bona fide* TM domain.[51,52]

We Are Currently Evaluating the Directionality of the Insertion of ATRAM into Membranes. Understanding which end of the peptide leads the membrane insertion is a prerequisite for employing ATRAM for therapeutic purposes. We hypothesize the ATRAM peptide will behave like the pHLIP, which inserts unidirectionally and fully translocates the C-terminal end across the membrane. This allows the pHLIP to deliver cargoes of different sizes and polarities across the membrane.[14] In case it is determined that the inserting end of the ATRAM peptide does not fully traverse the membrane, peptide design will be optimized to elongate the inserting end. A crucial feature of ATRAM is the use of multiple glutamic acid residues,[57,58] as the negative charges provide pH-sensing capability. Conveniently for our purposes, the pK_a values of acidic groups in hydrophobic environments are typically higher than when they are hydrated.[58,59] Hence, while a Glu side chain has a pK_a of ~4.0 in solution, values as high as 8.8 have been reported for Glu in different environments.[60] It is then not surprising that the pK of ATRAM resulting from the titration of Glu was 6.5, while it is 6.0 for pHLIP. In fact, the half-unit pK difference between ATRAM and pHLIP corresponds to the pK_a difference between Glu and Asp in solution. The side chain of Glu also increases the water solubility of the ATRAM peptide, as a result of its low hydrophobicity.

The design of membrane peptides is often complicated by their disruption of lipid bilayers. For example, the GALA peptide, also rich in glutamic acids, has been shown to cause bilayer solubilization and membrane fusion.[28,61] Figure 2A shows that ATRAM does not cause fusion or hemifusion of POPC vesicles. We also performed leakage experiments to evaluate the integrity of the membrane, using pHLIP as a control for a nondisruptive peptide. Our data show that the leakage observed for pHLIP, while still small, was higher than the value previously reported.[33] We attribute these differences to the high sensitivity of our calcein assay, where the leakage value reported might be artifactually increased. For instance, in our hands, careful pipet sample mixing resulted in calcein leakage, maybe as a result of physically stressing the vesicles. Nevertheless, we observed similar calcein leakage for pHLIP and ATRAM except at the higher peptide concentration, 0.7 μM. If ATRAM did in fact significantly disrupt the integrity of membranes, we would expect it also to cause cell toxicity. However, viability studies in two different cell lines showed that ATRAM caused no toxicity, even at a concentration (2 μM) higher than that employed for the leakage assay, showing that the peptide is not toxic to cells in culture. FRET experiments also showed that ATRAM forms a TM oligomer in the membrane under acidic conditions (Figure 2E). The FRET data suggest the presence of dimers or trimers. We suggest that ATRAM might form a dimer, because it contains GxxxG domains, which have been identified to induce dimerization in numerous transmembrane domains.[62,63]

Two interesting works that describe different efforts to design peptides with pH-dependent membrane insertion have recently been published. The DeGrado group computationally designed a series of peptides and evaluated their ability to form pores in the membrane upon acidification.[64] Oligomeric assembly was achieved both in solution and in the presence of membranes, where the peripheral state was postulated to exchange into a transmembrane pore. The groups of Hristova and Wimley employed a different approach, decorating the lytic peptide melittin with different acidic residues.[65] While macromolecular release across the membrane was not achieved in this case, interestingly, the resulting peptides were able to form an α-helix in POPC vesicles in a pH-dependent fashion. However, the orientation of the helix was not determined, and the pK values were highly acidic, between 4.6 and 5.0.

Malignant solid tumors typically have an extracellular environment with a pH value of 6.5–6.9,[66] significantly more acidic than healthy tissues, where the extracellular pH is 7.2–

DOI: 10.1021/acs.biochem.5b00856
Biochemistry 2015, 54, 6567–6575

7.4.[6] Interestingly, the membrane insertion p*K* of the ATRAM peptide is 6.5, suggesting that it might be effective in targeting malignant solid tumors. Our data show that the targeting of cells by ATRAM is very efficient, and importantly, the level of targeting is significantly higher under acidic conditions (Figure 3). Interestingly, for the A375 melanoma cells, strong targeting was achieved at pH 5.0 and 6.0, suggesting that high acidity is not required for efficient cell targeting. It has been previously reported that the membrane insertion p*K* of pHLIP differs between cells with differing lipid compositions.[67] A similar behavior might account for the observed requirement of higher acidity for maximal ATRAM insertion in H358 cells (Figure 3B). Interestingly, for both cell lines, we observed a higher level of targeting by ATRAM than by pHLIP. This might be partially explained by the slightly higher lipid affinity of ATRAM. Hence, while the POPC partition coefficient, K_p, of ATRAM at pH 8 was $(5.5 \pm 2.5) \times 10^5$, the K_p of pHLIP obtained under identical conditions was $(2.1 \pm 0.4) \times 10^5$.[9] The targeting differences observed between the two cell lines might also be associated with the distinct cellular distribution for ATRAM. In H358 cells, ATRAM localizes primarily to the plasma membrane, while in A375 cells, it is also heterogeneously distributed across the cytoplasm, probably at endocytic vesicles. We observed a similar trend for pHLIP, in agreement with a previous suggestion that pHLIP might leave the plasma membrane because of membrane recycling and/or endocytosis.[50]

Here we show that ATRAM is soluble at high concentrations, at least up to 200 μM. This contrasts with the case for pHLIP, for which peptide aggregation is observed above 7 μM.[51] When membranes are available, ATRAM binds to the bilayer surface, adopting a partially helical structure that lies parallel to the membrane plane. Finally, acidity drives ATRAM to insert, forming a transmembrane helix, which increases its affinity for membranes. The POPC insertion p*K* of ATRAM was 6.5, suggesting that ATRAM might be able to target the more frequent mildly acidic diseased tissues. The observed lack of cellular toxicity and the efficient targeting of cells in an acidity-dependent fashion suggest that ATRAM might be a promising new tool for targeted therapies applied to cancer and other acidic diseases.

AUTHOR INFORMATION

Corresponding Author

*E-mail: fbarrera@utk.edu. Telephone: (865) 974-4496. Fax.: (865) 974-6306.

Author Contributions

V.P.N., D.S.A., and H.L.S. designed, performed, and analyzed the experiments. F.L.D. performed and analyzed the experiments. F.N.B. designed and analyzed the research and conceived and coordinated the study. V.P.N., D.S.A., H.L.S., and F.N.B. wrote the paper. All authors reviewed the results and approved the final version of the manuscript.

Notes

The authors declare no competing financial interest.

ACKNOWLEDGMENTS

F.N.B. thanks Donald M. Engelman (Yale University, New Haven, CT) for numerous insightful discussions over the years. We also thank Jo Thota and Martina Little for performing the fluorescence solubility assay in buffer and Jose Antonio Poveda for advice on FRET experiments.

ABBREVIATIONS

CD, circular dichroism; LUVs, large unilamellar vesicles; NBD, nitrobenzoxadiazole; OCD, oriented circular dichroism; POPC, 1-palmitoyl-2-oleoyl-*sn*-glycero-3-phosphocholine; TM, transmembrane.

REFERENCES

(1) Yamaguchi, H., Chang, S. S., Hsu, J. L., and Hung, M. C. (2014) Signaling cross-talk in the resistance to HER family receptor targeted therapy. *Oncogene 33*, 1073−1081.

(2) Schornack, P. A., and Gillies, R. J. (2003) Contributions of cell metabolism and H+ diffusion to the acidic pH of tumors. *Neoplasia 5*, 135−145.

(3) Schulze, A., and Harris, A. L. (2012) How cancer metabolism is tuned for proliferation and vulnerable to disruption. *Nature 491*, 364−373.

(4) Vander Heiden, M. G., Cantley, L. C., and Thompson, C. B. (2009) Understanding the Warburg effect: the metabolic requirements of cell proliferation. *Science 324*, 1029−1033.

(5) Martinez-Outschoorn, U. E., Prisco, M., Ertel, A., Tsirigos, A., Lin, Z., Pavlides, S., Wang, C., Flomenberg, N., Knudsen, E. S., Howell, A., Pestell, R. G., Sotgia, F., and Lisanti, M. P. (2011) Ketones and lactate increase cancer cell "stemness," driving recurrence, metastasis and poor clinical outcome in breast cancer: achieving personalized medicine via Metabolo-Genomics. *Cell Cycle 10*, 1271−1286.

(6) Estrella, V., Chen, T., Lloyd, M., Wojtkowiak, J., Cornnell, H. H., Ibrahim-Hashim, A., Bailey, K., Balagurunathan, Y., Rothberg, J. M., Sloane, B. F., Johnson, J., Gatenby, R. A., and Gillies, R. J. (2013) Acidity generated by the tumor microenvironment drives local invasion. *Cancer Res. 73*, 1524−1535.

(7) Gottfried, E., Kreutz, M., and Mackensen, A. (2012) Tumor metabolism as modulator of immune response and tumor progression. *Semin. Cancer Biol. 22*, 335−341.

(8) Fosgerau, K., and Hoffmann, T. (2015) Peptide therapeutics: current status and future directions. *Drug Discovery Today 20*, 122−128.

(9) Scott, H. L., Nguyen, V. P., Alves, D. S., Davis, F. L., Booth, K. R., Bryner, J., and Barrera, F. N. (2015) The Negative Charge of the Membrane Has Opposite Effects on the Membrane Entry and Exit of pH-Low Insertion Peptide. *Biochemistry 54*, 1709−1712.

(10) Ladokhin, A. S., Jayasinghe, S., and White, S. H. (2000) How to measure and analyze tryptophan fluorescence in membranes properly, and why bother? *Anal. Biochem. 285*, 235−245.

(11) Moon, C. P., and Fleming, K. G. (2011) Using tryptophan fluorescence to measure the stability of membrane proteins folded in liposomes. *Methods Enzymol. 492*, 189−211.

(12) Hunt, J. F., Rath, P., Rothschild, K. J., and Engelman, D. M. (1997) Spontaneous, pH-dependent membrane insertion of a transbilayer alpha-helix. *Biochemistry 36*, 15177−15192.

(13) Andreev, O. A., Engelman, D. M., and Reshetnyak, Y. K. (2014) Targeting diseased tissues by pHLIP insertion at low cell surface pH. *Front. Physiol. 5*, 97.

(14) Deacon, J. C., Engelman, D. M., and Barrera, F. N. (2015) Targeting acidity in diseased tissues: Mechanism and applications of the membrane-inserting peptide, pHLIP. *Arch. Biochem. Biophys. 565*, 40−48.

(15) Andreev, O. A., Karabadzhak, A. G., Weerakkody, D., Andreev, G. O., Engelman, D. M., and Reshetnyak, Y. K. (2010) pH (low) insertion peptide (pHLIP) inserts across a lipid bilayer as a helix and exits by a different path. *Proc. Natl. Acad. Sci. U. S. A. 107*, 4081−4086.

(16) Snider, C., Jayasinghe, S., Hristova, K., and White, S. H. (2009) MPEx: a tool for exploring membrane proteins. *Protein Sci. 18*, 2624−2628.

(17) Liu, L. P., and Deber, C. M. (1999) Combining hydrophobicity and helicity: a novel approach to membrane protein structure prediction. *Bioorg. Med. Chem. 7*, 1−7.

DOI: 10.1021/acs.biochem.5b00856
Biochemistry 2015, 54, 6567−6575

(18) Liu, L. P., and Deber, C. M. (1998) Guidelines for membrane protein engineering derived from de novo designed model peptides. *Biopolymers 47*, 41−62.
(19) van Meer, G., and de Kroon, A. I. (2011) Lipid map of the mammalian cell. *J. Cell Sci. 124*, 5−8.
(20) van Meer, G., Voelker, D. R., and Feigenson, G. W. (2008) Membrane lipids: where they are and how they behave. *Nat. Rev. Mol. Cell Biol. 9*, 112−124.
(21) Shai, Y. (1999) Mechanism of the binding, insertion and destabilization of phospholipid bilayer membranes by alpha-helical antimicrobial and cell non-selective membrane-lytic peptides. *Biochim. Biophys. Acta, Biomembr. 1462*, 55−70.
(22) Pucadyil, T. J., Mukherjee, S., and Chattopadhyay, A. (2007) Organization and dynamics of NBD-labeled lipids in membranes analyzed by fluorescence recovery after photobleaching. *J. Phys. Chem. B 111*, 1975−1983.
(23) Chattopadhyay, A. (1990) Chemistry and biology of N-(7-nitrobenz-2-oxa-1,3-diazol-4-yl)-labeled lipids: fluorescent probes of biological and model membranes. *Chem. Phys. Lipids 53*, 1−15.
(24) Kelly, S. M., and Price, N. (2000) The use of Circular Dichroism in the investigation of protein structure and function. *Curr. Protein Pept. Sci. 1*, 349−384.
(25) Fletcher, J. M., Harniman, R. L., Barnes, F. R. H., Boyle, A. L., Collins, A., Mantell, J., Sharp, T. H., Antognozzi, M., Booth, P. J., Linden, N., Miles, M. J., Sessions, R. B., Verkade, P., and Woolfson, D. N. (2013) Self-assembling cages from coiled-coil peptide modules. *Science 340*, 595−599.
(26) Wu, Y., Huang, H. W., and Olah, G. A. (1990) Method of oriented circular dichroism. *Biophys. J. 57*, 797−806.
(27) Ulmschneider, M. B., Ulmschneider, J. P., Schiller, N., Wallace, B. A., von Heijne, G., and White, S. H. (2014) Spontaneous transmembrane helix insertion thermodynamically mimics translocon-guided insertion. *Nat. Commun. 5*, 4863.
(28) Li, W., Nicol, F., and Szoka, F. C., Jr. (2004) GALA: a designed synthetic pH-responsive amphipathic peptide with applications in drug and gene delivery. *Adv. Drug Delivery Rev. 56*, 967−985.
(29) Johnson, R. M., Harrison, S. D., and Maclean, D. (2011) Therapeutic applications of cell-penetrating peptides. *Methods Mol. Biol. 683*, 535−551.
(30) Lindberg, S., Copolovici, D. M., and Langel, U. (2011) Therapeutic delivery opportunities, obstacles and applications for cell-penetrating peptides. *Ther. Delivery 2*, 71−82.
(31) Foged, C., and Nielsen, H. M. (2008) Cell-penetrating peptides for drug delivery across membrane barriers. *Expert Opin. Drug Delivery 5*, 105−117.
(32) Mangoni, M. L., and Shai, Y. (2011) Short native antimicrobial peptides and engineered ultrashort lipopeptides: similarities and differences in cell specificities and modes of action. *Cell. Mol. Life Sci. 68*, 2267−2280.
(33) Zoonens, M., Reshetnyak, Y. K., and Engelman, D. M. (2008) Bilayer interactions of pHLIP, a peptide that can deliver drugs and target tumors. *Biophys. J. 95*, 225−235.
(34) Rausell, C., Munoz-Garay, C., Miranda-CassoLuengo, R., Gomez, I., Rudino-Pinera, E., Soberon, M., and Bravo, A. (2004) Tryptophan spectroscopy studies and black lipid bilayer analysis indicate that the oligomeric structure of Cry1Ab toxin from Bacillus thuringiensis is the membrane-insertion intermediate. *Biochemistry 43*, 166−174.
(35) Gerber, D., and Shai, Y. (2000) Insertion and organization within membranes of the delta-endotoxin pore-forming domain, helix 4-loop-helix 5, and inhibition of its activity by a mutant helix 4 peptide. *J. Biol. Chem. 275*, 23602−23607.
(36) Cheng, C. J., Bahal, R., Babar, I. A., Pincus, Z., Barrera, F., Liu, C., Svoronos, A., Braddock, D. T., Glazer, P. M., Engelman, D. M., Saltzman, W. M., and Slack, F. J. (2014) MicroRNA silencing for cancer therapy targeted to the tumour microenvironment. *Nature 518*, 107−110.
(37) Reshetnyak, Y. K., Yao, L., Zheng, S., Kuznetsov, S., Engelman, D. M., and Andreev, O. A. (2011) Measuring tumor aggressiveness and targeting metastatic lesions with fluorescent pHLIP. *Mol. Imaging Biol. 13*, 1146−1156.
(38) Perez-Aguilar, J. M., and Saven, J. G. (2012) Computational design of membrane proteins. *Structure (Oxford, U. K.) 20*, 5−14.
(39) Senes, A. (2011) Computational design of membrane proteins. *Curr. Opin. Struct. Biol. 21*, 460−466.
(40) Baker, D. (2014) Centenary Award and Sir Frederick Gowland Hopkins Memorial Lecture. Protein folding, structure prediction and design. *Biochem. Soc. Trans. 42*, 225−229.
(41) Barth, P., Schonbrun, J., and Baker, D. (2007) Toward high-resolution prediction and design of transmembrane helical protein structures. *Proc. Natl. Acad. Sci. U. S. A. 104*, 15682−15687.
(42) Yin, H., Slusky, J. S., Berger, B. W., Walters, R. S., Vilaire, G., Litvinov, R. I., Lear, J. D., Caputo, G. A., Bennett, J. S., and DeGrado, W. F. (2007) Computational design of peptides that target transmembrane helices. *Science 315*, 1817−1822.
(43) Joh, N. H., Wang, T., Bhate, M. P., Acharya, R., Wu, Y., Grabe, M., Hong, M., Grigoryan, G., and DeGrado, W. F. (2014) De novo design of a transmembrane Zn^{+}-transporting four-helix bundle. *Science 346*, 1520−1524.
(44) Korendovych, I. V., Senes, A., Kim, Y. H., Lear, J. D., Fry, H. C., Therien, M. J., Blasie, J. K., Walker, F. A., and Degrado, W. F. (2010) De novo design and molecular assembly of a transmembrane diporphyrin-binding protein complex. *J. Am. Chem. Soc. 132*, 15516−15518.
(45) Lichtenstein, B. R., Farid, T. A., Kodali, G., Solomon, L. A., Anderson, J. L. R., Sheehan, M. M., Ennist, N. M., Fry, B. A., Chobot, S. E., Bialas, C., Mancini, J. A., Armstrong, C. T., Zhao, Z., Esipova, T. V., Snell, D., Vinogradov, S. A., Discher, B. M., Moser, C. C., and Dutton, P. L. (2012) Engineering oxidoreductases: maquette proteins designed from scratch. *Biochem. Soc. Trans. 40*, 561−566.
(46) Lear, J. D., Wasserman, Z. R., and DeGrado, W. F. (1988) Synthetic amphiphilic peptide models for protein ion channels. *Science 240*, 1177−1181.
(47) Slivka, P. F., Wong, J., Caputo, G. A., and Yin, H. (2008) Peptide probes for protein transmembrane domains. *ACS Chem. Biol. 3*, 402−411.
(48) Viola-Villegas, N. T., Carlin, S. D., Ackerstaff, E., Sevak, K. K., Divilov, V., Serganova, I., Kruchevsky, N., Anderson, M., Blasberg, R. G., Andreev, O. A., Engelman, D. M., Koutcher, J. A., Reshetnyak, Y. K., and Lewis, J. S. (2014) Understanding the pharmacological properties of a metabolic PET tracer in prostate cancer. *Proc. Natl. Acad. Sci. U. S. A. 111*, 7254−7259.
(49) Burns, K. E., Robinson, M. K., and Thevenin, D. (2015) Inhibition of Cancer Cell Proliferation and Breast Tumor Targeting of pHLIP-Monomethyl Auristatin E Conjugates. *Mol. Pharmaceutics 12*, 1250−1258.
(50) Onyango, J. O., Chung, M. S., Eng, C.-H., Klees, L. M., Langenbacher, R., Yao, L., and An, M. (2015) Noncanonical Amino Acids to Improve the pH Response of pHLIP Insertion at Tumor Acidity. *Angew. Chem., Int. Ed. 54*, 3658−3663.
(51) Reshetnyak, Y. K., Segala, M., Andreev, O. A., and Engelman, D. M. (2007) A monomeric membrane peptide that lives in three worlds: in solution, attached to, and inserted across lipid bilayers. *Biophys. J. 93*, 2363−2372.
(52) Weerakkody, D., Moshnikova, A., Thakur, M. S., Moshnikova, V., Daniels, J., Engelman, D. M., Andreev, O. A., and Reshetnyak, Y. K. (2013) Family of pH (low) insertion peptides for tumor targeting. *Proc. Natl. Acad. Sci. U. S. A. 110*, 5834−5839.
(53) Musial-Siwek, M., Karabadzhak, A., Andreev, O. A., Reshetnyak, Y. K., and Engelman, D. M. (2010) Tuning the insertion properties of pHLIP. *Biochim. Biophys. Acta, Biomembr. 1798*, 1041−1046.
(54) White, S. H., and Wimley, W. C. (1999) Membrane protein folding and stability: Physical principles. *Annu. Rev. Biophys. Biomol. Struct. 28*, 319−365.
(55) Jaud, S., Fernandez-Vidal, M., Nilsson, I., Meindl-Beinker, N. M., Hubner, N. C., Tobias, D. J., von Heijne, H. G., and White, S. H. (2009) Insertion of short transmembrane helices by the Sec61 translocon. *Proc. Natl. Acad. Sci. U. S. A. 106*, 11588−11593.

DOI: 10.1021/acs.biochem.5b00856
Biochemistry 2015, 54, 6567−6575

(56) Greenfield, N. J. (2007) Using circular dichroism spectra to estimate protein secondary structure. *Nat. Protoc 1*, 2876−2890.
(57) London, E., and Shahidullah, K. (2009) Transmembrane vs. non-transmembrane hydrophobic helix topography in model and natural membranes. *Curr. Opin. Struct. Biol. 19*, 464−472.
(58) Caputo, G. A., and London, E. (2004) Position and ionization state of Asp in the core of membrane-inserted alpha helices control both the equilibrium between transmembrane and nontransmembrane helix topography and transmembrane helix positioning. *Biochemistry 43*, 8794−8806.
(59) Harms, M. J., Castaneda, C. A., Schlessman, J. L., Sue, G. R., Isom, D. G., Cannon, B. R., and Garcia-Moreno E., B. (2009) The pK(a) values of acidic and basic residues buried at the same internal location in a protein are governed by different factors. *J. Mol. Biol. 389*, 34−47.
(60) Pace, C. N., Grimsley, G. R., and Scholtz, J. M. (2009) Protein ionizable groups: pK values and their contribution to protein stability and solubility. *J. Biol. Chem. 284*, 13285−13289.
(61) Parente, R. A., Nir, S., and Szoka, F. C., Jr. (1988) pH-dependent fusion of phosphatidylcholine small vesicles. Induction by a synthetic amphipathic peptide. *J. Biol. Chem. 263*, 4724−4730.
(62) Senes, A., Engel, D. E., and DeGrado, W. F. (2004) Folding of helical membrane proteins: the role of polar, GxxxG-like and proline motifs. *Curr. Opin. Struct. Biol. 14*, 465−479.
(63) Russ, W. P., and Engelman, D. M. (2000) The GxxxG motif: a framework for transmembrane helix-helix association. *J. Mol. Biol. 296*, 911−919.
(64) Zhang, Y., Bartz, R., Grigoryan, G., Bryant, M., Aaronson, J., Beck, S., Innocent, N., Klein, L., Procopio, W., Tucker, T., Jadhav, V., Tellers, D. M., and DeGrado, W. F. (2015) Computational Design and Experimental Characterization of Peptides Intended for pH-Dependent Membrane Insertion and Pore Formation. *ACS Chem. Biol. 10*, 1082−1093.
(65) Wiedman, G., Wimley, W. C., and Hristova, K. (2015) Testing the limits of rational design by engineering pH sensitivity into membrane-active peptides. *Biochim. Biophys. Acta, Biomembr. 1848*, 951−957.
(66) van Sluis, R., Bhujwalla, Z. M., Raghunand, N., Ballesteros, P., Alvarez, J., Cerdan, S., Galons, J. P., and Gillies, R. J. (1999) In vivo imaging of extracellular pH using 1H MRSI. *Magn. Reson. Med. 41*, 743−750.
(67) Barrera, F. N., Fendos, J., and Engelman, D. M. (2012) Membrane physical properties influence transmembrane helix formation. *Proc. Natl. Acad. Sci. U. S. A. 109*, 14422−14427.
(68) Kyrychenko, A., Vasquez-Montes, V., Ulmschneider, M. B., and Ladokhin, A. S. (2015) Lipid headgroups modulate membrane insertion of pHLIP peptide. *Biophys. J. 108*, 791−794.
(69) Wolber, P. K., and Hudson, B. S. (1979) An analytic solution to the Forster energy transfer problem in two dimensions. *Biophys. J. 28*, 197−210.

DOI: 10.1021/acs.biochem.5b00856
Biochemistry 2015, 54, 6567−6575